

FunPhase: A Periodic Functional Autoencoder for Motion Generation via Phase Manifolds

Marco Pegoraro Autodesk Research marco.pegoraro@ist.ac.at	Evan Atherton Autodesk Research evan.atherton@autodesk.com	Bruno Roy Autodesk Research bruno.roy@autodesk.com
Aliasghar Khani Autodesk Research aliasghar.khani@autodesk.com		Arianna Rampini Autodesk Research arianna.rampini@autodesk.com

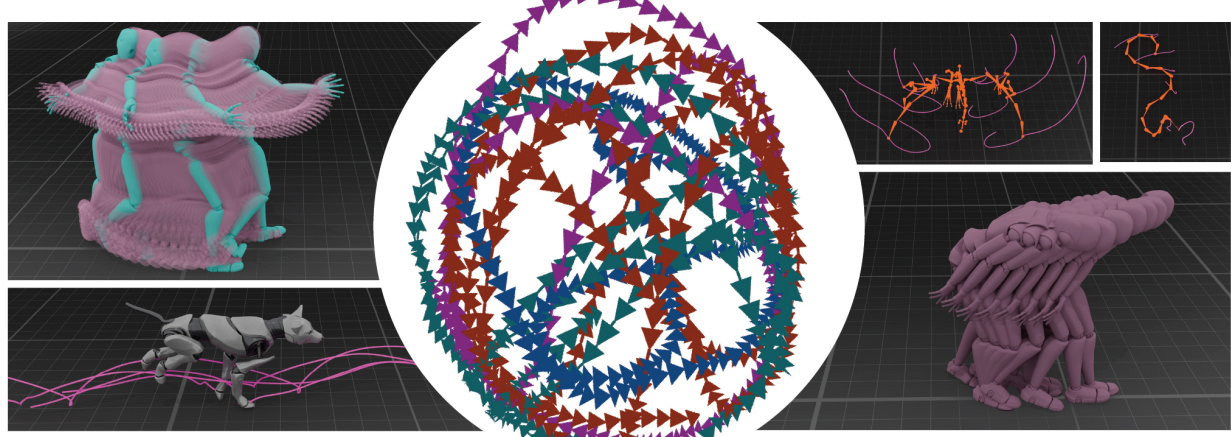


Figure 1. FunPhase is a functional periodic autoencoder that learns a phase-structured manifold for motion, enabling smooth, continuous spatio-temporal reconstruction, and skeleton-agnostic motion prediction and generation.

Abstract

Learning natural body motion remains challenging due to the strong coupling between spatial geometry and temporal dynamics. Embedding motion in phase manifolds, latent spaces that capture local periodicity, has proven effective for motion prediction; however, existing approaches lack scalability and remain confined to specific settings. We introduce FunPhase, a functional periodic autoencoder that learns a phase manifold for motion and replaces discrete temporal decoding with a function-space formulation, enabling smooth trajectories that can be sampled at arbitrary temporal resolutions. FunPhase supports downstream tasks such as super-resolution and partial-body motion completion, generalizes across skeletons and datasets, and unifies motion prediction and generation within a single interpretable manifold. Our model achieves substantially lower

reconstruction error than prior periodic autoencoder baselines while enabling a broader range of applications and performing on par with state-of-the-art motion generation methods.

1. Introduction

Motion generation refers to the task of synthesizing realistic and coherent sequences of human or character movements, typically represented as 3D joint trajectories or poses, based on diverse inputs such as action labels, textual descriptions, or environmental cues. This capability is central to computer vision, computer graphics, robotics, and human-computer interaction, with applications spanning virtual avatar animation, video games, and embodied agents [13]. Effective motion generation automates traditionally manual

and time-intensive animation processes, while also enabling behavioral modeling, simulation, and data augmentation.

Despite recent progress in generative modeling, learning motion remains a challenging problem due to the complex coupling between spatial geometry and temporal dynamics [30]. Generic diffusion or autoregressive models that excel in visual and language domains often fail to produce physically plausible results. The difficulty arises from the sparsity and highly nonlinear structure of the motion space, which can lead to artifacts such as root drift, inconsistent contacts, or temporal jitter [39].

A promising direction to address these issues is the use of *phase representations*, which encode the temporal progression of motion in a compact, interpretable form [26]. Recent work, such as *DeepPhase* [26], shows that phase-aware representations significantly improve motion alignment and prediction. However, existing models remain limited in scalability, restricted to fixed skeletons, and are not easily extensible to probabilistic or generative frameworks.

Our idea in this research is to extend the learned manifold framework to an expressive space compatible with modern generative models and capable of representing diverse datasets. We introduce **FunPhase**, a *functional periodic autoencoder* that learns a phase manifold for motion while reconstructing motion as a continuous spatio-temporal function rather than a discrete frame sequence. This functional formulation not only produces smooth trajectories that can be sampled at arbitrary temporal resolutions but also provides a natural interface for integrating physics priors [31], which are of fundamental importance in the motion domain [35]. Moreover, it scales across heterogeneous skeletons and unifies motion prediction and generation within a single interpretable framework. Our architecture builds upon the functional generative framework [31], while preserving the interpretability of phase decomposition introduced in DeepPhase [26].

The main contributions of this work are summarized as follows:

1. We propose **FunPhase**, a functional extension of the Periodic Autoencoder that reconstructs motion as a spatio-temporal function while preserving a meaningful phase manifold;
2. We demonstrate the versatility of FunPhase across downstream tasks, including motion super-resolution and partial-body motion completion;
3. We introduce a proof-of-concept *Neural Motion Controller* operating in the learned phase manifold, enabling phase-aligned and temporally consistent control;
4. We employ FunPhase latents for *motion generation via diffusion in functional space*, achieving state-of-the-art performance on standard benchmarks. We further show that phase features substantially improve denoising stability and generation quality over baseline models.

Overall, FunPhase bridges structured kinematic modeling with modern generative methods, providing a unified, skeleton-agnostic framework for learning, predicting, and generating motion functions.

2. Related Work

Phase in Motion Synthesis and Control. Methods that represent motion in the frequency domain date back to the 1990s, including early work on motion synthesis [16] and editing [1]. With the advent of machine learning, phase-based representations have been widely adopted to improve temporal alignment and controllability in motion models. The *Phase-Functioned Neural Network (PFNN)* [9] introduced a phase-conditioned architecture for locomotion control, where network weights are modulated by a scalar phase inferred from foot contacts. Subsequent extensions [24, 25] generalized this idea to multi-contact and limb-specific phase conditioning. *DeepPhase* [26] further extended the concept to unstructured motion data by learning multi-dimensional phase variables, forming a phase manifold that captures complex periodic relationships. Follow-up works explored phase-based in-betweening [23] and group choreography modeling [14]. Recent approaches such as *Walk-TheDog* [15] apply phase-space vector quantization with a shared motion vocabulary across species. Despite their effectiveness, these methods remain task-specific, limited in scalability, and not probabilistic, not allowing generative motion synthesis. Our approach directly overcomes these limitations by introducing a functional phase manifold that is both generative and skeleton-agnostic, while retaining the interpretability of phase-based representations.

Motion Generative Models. While a few studies have explored generation in phase space, such as *PhaseDiff* [29], most approaches transfer existing generative paradigms directly to motion without domain-specific adaptations. Notable examples include diffusion-based models such as *MDM* [27] and latent diffusion models such as *MLD* [3], as well as autoregressive approaches like *MotionGPT* [11]. A wide range of follow-up works have focused on scaling to larger datasets and models [4, 34], yet common issues persist, including implausible foot contacts and limited controllability. *PhaseDiff*, while incorporating phase information, suffers from poor generation quality and lack of high frequency. Controllable human motion generation has been further explored in *CAMDM* [2], which employs motion diffusion probabilistic models to produce diverse character animations that respond in real time to dynamic user control signals. Efforts toward generalization across skeletons include *AnyTop* [6], *AniMo* [32], *UniMoGen* [12], and *SinMDM* [20]. *SinMDM* learns the internal motifs of a single motion sequence with arbitrary topology, enabling long and diverse animations across humans, animals, and imaginary creatures. Most recently, *ACMDM* [18] showed that repre-

senting motion with absolute joint coordinates can achieve state-of-the-art fidelity and diversity.

Comprehensive surveys [13, 39] review these advances, emphasizing the growing need for interpretable and temporally structured motion priors. Notably, all the above are *frame-based* approaches, whereas our model reconstructs motion as a *spatio-temporal function*, allowing variable-rate decoding and improved stability. Moreover, we show that incorporating phase features provides an effective inductive bias that regularizes the generative process and drastically improves denoising stability.

Generative Models over Function Space. Early attempts at generating function spaces [5] demonstrated the potential of representing data as continuous mappings, including applications in domains such as biological processes [33]. More recently, *FunDiff* [31] formalized diffusion over function space, enabling smooth and resolution-independent generative modeling. Their formulation provides natural regularization and compatibility with physical priors, properties that are particularly useful for motion generation. Our work draws inspiration from this functional perspective: FunPhase extends the concept to motion data, combining phase-manifold learning with a functional decoder for smooth, skeleton-agnostic motion synthesis.

3. Background

The use of phase variables to describe motion progression has been well established in data-driven motion modeling, most notably in the *Phase-Functioned Neural Network* (PFNN) [9] and its extensions to multi-contact and limb-specific phase representations [17, 25]. These methods rely on phase signals, often derived from contact heuristics, to align frames across motion sequences. Building upon this idea, *DeepPhase* [26] introduced the concept of a *motion phase manifold*, which generalizes phase modeling to unstructured motion data.

3.1. The Motion Phase Manifold

DeepPhase proposed to learn multi-dimensional phase variables directly from motion data through an encoder-based latent space endowed with a frequency-domain inductive bias. The so-called *Periodic Autoencoder* (PAE) models the temporal structure of motion as a combination of learned periodic components.

Given an input motion sequence $\mathbf{X} \in \mathbb{R}^{D \times N}$, where D is the number of motion features and N is the number of frames, the encoder g maps the sequence into a latent representation $L = g(\mathbf{X}) \in \mathbb{R}^{M \times N}$ with M latent channels using $1D$ convolution. Each latent channel \hat{l}_c is then parameterized as a sinusoidal function:

$$\hat{l}_c = a_c \cdot \sin(2\pi(f_c \cdot \mathcal{T} - s_c)) + b_c \in \mathbb{R}^4, \quad (1)$$

where a_c, f_c, s_c, b_c denote amplitude, frequency, phase shift, and offset, respectively, and \mathcal{T} is the time window. The parameters a_c, f_c, b_c are obtained via a differentiable real-valued Fast Fourier Transform (FFT) layer, while s_c is predicted through a learned phase regressor. This formulation enforces each latent channel to capture locally periodic motion components, such as gait cycles, arm swings, or torso oscillations. Finally, the decoder reconstructs the original motion through $1D$ deconvolutions $\mathbf{Y} = h([\hat{l}_1, \dots, \hat{l}_M])$, minimizing the mean-squared error loss between input and output.

From the periodic parameters, a *phase manifold* $\mathcal{P}(t) \in \mathbb{R}^{2M}$ is constructed:

$$\mathcal{P}_{2i-1}^{(t)} = a_i^{(t)} \cdot \sin(2\pi \cdot s_i^{(t)}), \quad (2)$$

$$\mathcal{P}_{2i}^{(t)} = a_i^{(t)} \cdot \cos(2\pi \cdot s_i^{(t)}). \quad (3)$$

This hyperspherical transformation couples amplitude and phase while discarding quasi-static parameters such as frequency and offset.

3.2. Interpretation

As discussed in [26], this formulation promotes clustering of motions both in space and time, yielding a smooth and interpretable manifold where temporal alignment emerges naturally. The learned phase manifold $\mathcal{P}^{(t)}$ captures the rhythmic structure of motion across multiple body parts, forming smooth cyclic trajectories in low-dimensional projections (Figure 3). This representation facilitates downstream tasks such as motion matching, style transfer, and phase-based motion synthesis.

However, the original DeepPhase framework is inherently limited by its *frame-based convolutional* design and dependency on a *fixed skeleton topology*, which constrains scalability and generalization across datasets. Moreover, extending the model to probabilistic or generative settings, where one needs to sample from a learned motion distribution, is non-trivial.

In the following section, we build on these insights and introduce **FunPhase**, a functional extension of the Periodic Autoencoder. FunPhase reconstructs motion as a continuous spatio-temporal function rather than a discrete sequence, enabling scalable and skeleton-agnostic phase modeling suitable for generative motion synthesis.

4. Methods

Our motion generation framework comprises two stages, conceptually similar to latent diffusion pipelines. First, we introduce a Periodic Function Autoencoder (**FunPhase**) that learns a continuous periodic representation of movement in function space. Our model maps discrete motion sequences to a compact latent space parameterized by periodic functions, enabling motion reconstruction and

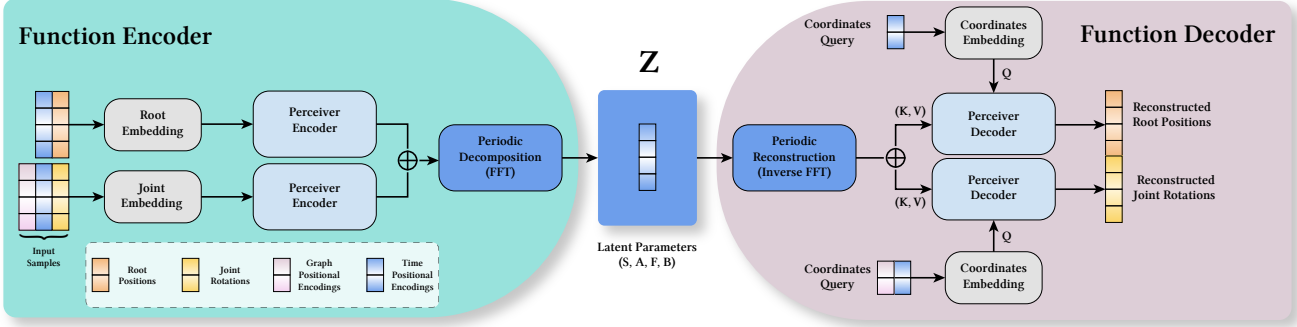


Figure 2. **Overview of the Periodic Function Autoencoder (FunPhase) architecture.** The figure illustrates the separated processing of joint rotations and root positions through Perceiver-based encoder–decoder modules. The latent space is decomposed by a Fast Fourier Transform (FFT) layer in its periodic components (Phase shift, Amplitude, Frequency, Bias) to achieve an even more compact representation and enforce periodicity. The latent space is then reconstructed with the inverse FFT, and the functions are evaluated at the coordinates given as input to the decoder.

sampling at arbitrary temporal resolutions and facilitating downstream tasks such as motion synthesis and completion. The architecture of FunPhase is summarized in Figure 2 and described in detail in subsection 4.1. Second, we train a diffusion model operating in the learned phase manifold, as detailed in subsection 4.2. This stage enables probabilistic motion synthesis in the same functional space, producing temporally coherent and physically plausible motion trajectories.

4.1. FunPhase architecture

For our FunPhase design, we draw inspiration from the Fun-Diff architecture [31]. Our network is specifically adapted to model temporal sequences over a 3D skeletal graph.

Motion representation. We represent joint rotations using the continuous 6D rotation representation [38], which avoids the discontinuities and ambiguities inherent in other rotation parameterizations such as Euler angles or quaternions. For a skeleton with J joints, the motion at frame t is represented by a tensor of joint rotations $\mathbf{R}_t \in \mathbb{R}^{J \times 6}$. The root joint position is treated separately from the rotational components to decouple global translation from local articulation. Root positions are represented in world coordinates as $\mathbf{X}_t^{root} \in \mathbb{R}^3$, encoding the 3D location of the pelvis or root joint at each frame.

Positional Encoding. To provide the model with information about temporal structure and skeletal topology, we employ two types of positional encodings:

(i) *Temporal Encoding*: temporal coordinates are mapped using Fourier features with a fixed range of frequencies.

(ii) *Spatial Encoding*: skeletal structure is encoded using graph-based positional features derived from the Laplacian of the skeleton graph. For datasets with variable skeletal sizes, we instead use a heat-diffusion–based encoding that

captures multi-scale structural information.

Full mathematical details are provided in the Supplementary Materials.

Encoder. We employ separate encoding pathways for joint rotations and root positions, each with dedicated Perceiver-based encoders [10]. This architectural choice captures the distinct dynamics of global translation and local articulation. The *joint* encoder processes the concatenation of joint rotations and spatial-temporal positional encodings $\mathbf{h}_t^{joints} = [\mathbf{R}_t, \mathbf{p}^{graph}, \mathbf{p}_t^{time}]$. The Perceiver encoder consists of cross-attention blocks followed by self-attention blocks. It learns a set of L_{joints} latent tokens $\mathbf{Z}^{joints} \in \mathbb{R}^{L_{joints} \times d_{joints}}$ that attend to the input sequence via cross-attention:

$$\mathbf{Z}^{joints} = \text{PerceiverEnc}^{joints}(\mathbf{h}_{1:T}^{joints})$$

Similarly, the *root* encoder processes root positions concatenated with temporal encodings $\mathbf{h}^{root} = [\mathbf{X}_t^{root}, \mathbf{p}_t^{time}]$, producing latent tokens $\mathbf{Z}^{root} \in \mathbb{R}^{L_{root} \times d_{root}}$.

The joint and root latents are independently projected to a common dimensionality d_{latent} via linear layers, then concatenated and passed through a 1D convolutional bottleneck with circular padding to produce the unified latent representation:

$$\mathbf{Z} = \text{Conv1D}([\mathbf{Z}^{joints}; \mathbf{Z}^{root}]) \in \mathbb{R}^{C \times d_{latent}}$$

where C is the number of latent channels.

Phase Decomposition integration. The FunPhase framework enables channel-wise periodic decomposition following the DeepPhase approach [26]. Following their Periodic Autoencoder, we use a combination of the Fast Fourier Transform and a linear layer to obtain the periodic parameters, modeling each latent channel as a sinusoid.

Each latent channel is parameterized by four periodic components:

$$\boldsymbol{\theta}_c = [s_c, a_c, f_c, b_c] \in \mathbb{R}^4.$$

This compact representation encodes the complete periodic structure of motion in $4C$ parameters, where C ranges from 16 to 256 in our implementation, resulting in a compact representation with ≤ 1024 parameters per clip.

Decoder. The decoder reconstructs the latent function by evaluating the learned sinusoidal parameters (Equation 1). This reconstructed latent representation is then passed through the inverse bottleneck convolution and split into joint and root latents:

$$[\hat{\mathbf{Z}}^{joints}, \hat{\mathbf{Z}}^{root}] = \text{DeConv1D}(\hat{\mathbf{Z}})$$

The joint and root decoders use cross-attention to query the reconstructed latents at arbitrary spatio-temporal positions. For a query time t' and joint j' , the decoder produces:

$$\begin{aligned}\hat{\mathbf{R}}_{t',j'} &= \text{PerceiverDec}^{joints}(\hat{\mathbf{Z}}^{joints}, \mathbf{p}_{j'}^{graph}, \mathbf{p}_{t'}^{time}) \\ \hat{\mathbf{X}}_{t'}^{root} &= \text{PerceiverDec}^{root}(\hat{\mathbf{Z}}^{root}(t'), \mathbf{p}_{t'}^{time})\end{aligned}$$

This allows the model to sample motion at any temporal resolution, enabling applications like temporal super-resolution and motion retiming, and at any joint, enabling body completion.

Training Objective. The model is trained to minimize a combination of reconstruction losses:

(i) *Rotation Loss*: Geodesic distance for joint rotations:

$$\mathcal{L}_{rot} = \frac{1}{TJ} \sum_{t,j} \arccos \left(\frac{\text{tr}(\mathbf{R}_{t,j} \hat{\mathbf{R}}_{t,j}^\top) - 1}{2} \right) \quad (4)$$

(ii) *Root Position Loss*: Mean squared error for root positions:

$$\mathcal{L}_{root} = \|\mathbf{X}^{root} - \hat{\mathbf{X}}^{root}\|_2^2 \quad (5)$$

(iii) *Forward Kinematics Loss*: To enforce physical plausibility, we penalize deviations in forward-kinematics (FW) joint positions:

$$\mathcal{L}_{FK} = \|\text{FK}(\mathbf{R}, \mathbf{X}^{root}) - \text{FK}(\hat{\mathbf{R}}, \hat{\mathbf{X}}^{root})\|_2^2 \quad (6)$$

together with foot penetration (FP) and foot sliding (FS) penalties:

$$\mathcal{L}_{foot} = \|\text{FP}(\mathbf{R}, \mathbf{X}^{root}) - \text{FS}(\hat{\mathbf{R}}, \hat{\mathbf{X}}^{root})\|_2^2 \quad (7)$$

The total loss is:

$$\mathcal{L} = 0.5(\mathcal{L}_{rot} + \mathcal{L}_{root}) + 0.5(\mathcal{L}_{FK} + 0.01\mathcal{L}_{foot}) \quad (8)$$

The effectiveness of this composite loss and other design choices is validated in the Ablation section of the Supplementary materials.

4.2. Phase diffusion

Building upon the FunPhase autoencoder, we introduce a latent diffusion model that operates directly on the periodic function parameters, enabling class-conditional motion generation in a compact, semantically meaningful space.

Phase Transformation. The periodic parameterization $\boldsymbol{\theta}_c = [s_c, a_c, f_c, b_c]$ from FunPhase, while compact and interpretable, poses challenges for diffusion modeling due to the domain and distribution of some parameters. We apply domain transformations to ensure compatibility with Gaussian diffusion:

The phase $s_c \in [0, 1]$ is transformed to Cartesian coordinates to handle periodicity:

$$\begin{aligned}\mathbf{a}_c^{\cos} &= a_c \cos(2\pi s_c) \\ \mathbf{a}_c^{\sin} &= a_c \sin(2\pi s_c)\end{aligned}$$

This representation avoids discontinuities at the phase boundary and encodes both amplitude and phase information jointly.

The frequency $f_c \in [0, f_{max}]$ is unbounded via probit transformation:

$$f_c^{probit} = \sqrt{2} \cdot \text{erf}^{-1} \left(2 \cdot \frac{f_c}{f_{max}} - 1 \right)$$

where $f_{max} = 0.5 \cdot d_{latent}/(2\pi)$ and erf stands for the error function. This maps the bounded frequency domain to the entire real line \mathbb{R} , making it suitable for Gaussian noise injection.

The offset b_c is unbounded and requires no transformation. The final diffusion-compatible representation is:

$$\boldsymbol{\theta}_c^{diff} = [\mathbf{a}_c^{\cos}, \mathbf{a}_c^{\sin}, f_c^{probit}, b_c] \in \mathbb{R}^4 \quad (9)$$

After sampling, we recover the original periodic parameters:

$$\begin{aligned}a_c &= \sqrt{(\mathbf{a}_c^{\cos})^2 + (\mathbf{a}_c^{\sin})^2 + \epsilon} \\ s_c &= \frac{1}{2\pi} \arctan 2(\mathbf{a}_c^{\sin}, \mathbf{a}_c^{\cos}) \\ f_c &= f_{max} \cdot \frac{1}{2} \left(1 + \text{erf} \left(\frac{f_c^{probit}}{\sqrt{2}} \right) \right)\end{aligned}$$

In the Supplementary Materials, we provide a further analysis on the advantage of this choice.

Diffusion Model. We employ a Diffusion Transformer (DiT) [19] architecture adapted for 1D latent sequences. We use the *velocity parameterization*, in which the network predicts the instantaneous velocity field of the reverse diffusion process. This formulation provides more stable training and sampling compared to standard noise prediction [37]. At each timestep, the model outputs a velocity vector integrated with a linear noise schedule to obtain the latent trajectory. After sampling, we invert the latent transformations and decode motion using FunPhase. The model

is conditioned on class labels and partial motion inputs: known keyframes or joint rotations are encoded with the pretrained FunPhase encoder, and the resulting latents are concatenated with the class embedding.

Further architectural and diffusion details are provided in the Supplementary Materials.

5. Experiments

In this section, we first validate the proposed functional autoencoder (5.1), then demonstrate its applications to latent motion generation (5.2) and motion prediction (5.3). Finally, we present an ablation study of the main components of our method in the Ablation section of the Supplementary Materials.

Datasets. Our model is skeleton-agnostic and can be trained on datasets featuring a variety of characters. To demonstrate robustness and generalization, we evaluate it on both human and animal motion datasets. All sequences are divided into 60-frame windows (1 second each), unless otherwise specified.

- **100STYLE** [17]: Contains 100 distinct performative locomotion styles and over 4 million motion capture frames.
- **DOG** [36]: Dog motion capture dataset covering various locomotion modes such as walk, pace, and trot, as well as sitting, standing, and jumping, totaling approximately 30 minutes of motion.
- **TRUEBONES ZOO** [28]: A diverse collection of 70 animal skeletons, including quadrupeds, bipeds, insects, and flying birds, totaling 1,219 sequences (147,178 frames). We use the same preprocessing as [6] and we divided sequences into 30-frame windows (1 second each).

Metrics. Evaluating motion generation and reconstruction requires jointly assessing spatial accuracy, temporal coherence, physical plausibility, and perceptual realism [39]. Following standard practice, we employ a diverse set of metrics to ensure a fair and comprehensive evaluation.

- Reconstruction quality: *Joint Position Error (L2)*, *Geodesic Rotation Error* (Equation 4), and *Normalized Power Spectrum Similarity (NPSS)* [7].
- Physical plausibility: *Foot Sliding*, *Foot Penetration*, and acceleration-based smoothness (*Average Curve Length (ACL)*, *Coherence*).
- Generation quality: *Fréchet Inception Distance (FID)* and classification *Accuracy* using a pretrained motion classifier from [2], plus sample *Diversity*.
- Dataset-specific metrics: on TRUEBONES ZOO, we follow AnyTop [6] and report *Coverage* and motion diversity scores.

A full description of all metrics and implementation details is provided in the Supplementary Materials. Visual examples are provided in the supplemental video.

Baselines. We first compare our FunPhase model with

DeepPhase [26] on the reconstruction task using both 100STYLE and DOG datasets, and provide visual comparisons for the motion controller. To our knowledge, this is the first work to explore motion generation in a *function space*. Nevertheless, we compare with state-of-the-art latent diffusion approaches: the Absolute Coordinate Motion Diffusion Model (ACMDM) [18], the original Latent Motion Diffusion model (LDM) [3], and the Conditional Autoregressive Motion Diffusion Model (CAMDM) [2], which achieves state-of-the-art performance on stylized human locomotion (100STYLE). For multi-skeleton settings, we further compare with AnyTop [6] and SinMDM [20]. We use the released checkpoints for CAMDM, AnyTop, and retrain ACMDM and LDM on the 100STYLE dataset using their official code and settings. To further validate our autoencoder, we also compare the AE component of ACMDM and the VAE component of LDM against our FunPhase autoencoder. Finally, we include our Function Autoencoder without the phase component as an additional baseline for both reconstruction and generation tasks.

5.1. FunPhase

In this section, we assess the quality of the learned Phase Manifold and motion function in comparison with baseline models. We show that the Phase Manifold learned by our approach preserves the core behavior of DeepPhase while significantly improving the expressiveness and fidelity of motion reconstruction.

Learned Phase Manifold. We visualize the learned phase manifold and compare it against the one obtained with DeepPhase. After computing the phase manifold on running sequences from the DOG dataset, we extract the principal components (PCs) of the phase features and project them onto a 3D plane (Figure 3). For comparison, we compute the phase embeddings from DeepPhase and similarly project their PCs to 3D. We also visualize the PCs of the original motion features (root position and joint angles). We observe that our phase representation maintains a compact circular structure characteristic of cyclic motion, whereas the original motion features collapse into disorganized linear trajectories. This structured phase representation is known to be effective for downstream applications such as motion matching and control [26].

Reconstruction. To demonstrate that our model can accurately infer motion functions, we evaluate reconstruction error and physical plausibility of reconstructed motions, and compare FUNPHASE against baseline methods in Table 1. FUNPHASE substantially improves over DeepPhase in its ability to extract phase-aware motion representations, achieving lower reconstruction errors and consistently better physics-based scores. While ACMDM achieves slightly lower reconstruction errors, the regularizing effect of our phase decomposition leads to more physically consistent

Table 1. **Autoencoder comparison on the DOG and 100STYLE datasets.** FunPhase consistently outperforms DeepPhase in all metrics, showing more accurate and physically consistent reconstructions.

Dataset	Method	Position (cm) ↓	Orientation ↓	NPSS ↓	Sliding ↓	Penetration ↓	ACL ↓
DOG	DeepPhase -16C [26]	144	0.54	3.58	1.76	0.912	1.768
	FunPhase -16C	61.4	0.34	1.83	0.21	0.351	1.062
100STYLES	DeepPhase-32C [26]	92.9	0.35	3.68	1.47	0.414	1.504
	MLD-VAE [3]	59.8	0.29	2.93	0.88	0.211	1.380
	ACMDM-AE [18]	0.32	0.01	0.28	0.33	0.003	1.412
	Function AE-256C	0.74	<u>0.05</u>	<u>0.59</u>	0.23	0.001	1.383
	FunPhase -32C	1.93	0.10	1.18	0.16	<u>0.001</u>	1.371
	FunPhase -256C	<u>0.36</u>	0.20	0.75	<u>0.21</u>	0.001	<u>1.378</u>

Table 2. **Latent diffusion results on the 100STYLE dataset.** Comparison between FunPhase and state-of-the-art motion latent diffusion baselines. FID and Accuracy evaluate perceptual fidelity and condition alignment, respectively. Diversity measures pose variation across generated samples, while Foot Sliding, Coherence, and ACCL assess physical realism.

Method	FID ↓	Accuracy (%) ↑	Diversity ↑	Foot Sliding ↓	Coherence ↑	ACCL ↓
MLD [3]	1.99 ± 1.22	41.88	0.65 ± 0.01	1.16	1.06	1.34
ACMDM [18]	5.45 ± 3.04	15.67	0.75 ± 0.01	1.74	1.53	2.46
CAMDM [2]	0.91 ± 0.62	88.22	0.69 ± 0.01	<u>0.69</u>	1.08	6.02
Function Diff.	1.19 ± 0.43	34.27	0.54 ± 0.01	1.23	1.14	1.25
FunPhase	0.51 ± 0.16	<u>76.17</u>	0.64 ± 0.01	0.52	<u>1.17</u>	<u>1.33</u>

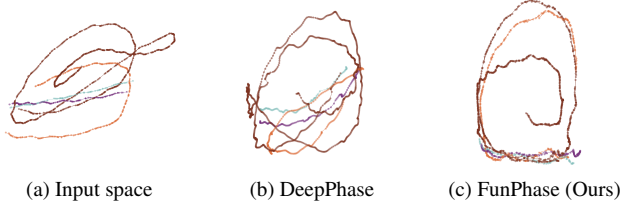


Figure 3. **Phase Manifold.** The plots show the phase manifolds obtained with DeepPhase and FunPhase, alongside the original motion features. All encoded sequences correspond to a dog-running motion.

results. Notably, despite operating in a more compact latent space imposed by the periodic parameterization, FUN-PHASE still surpasses the Function Autoencoder in reconstruction accuracy. This indicates that introducing a periodic component in the latent space does not compromise representational power; instead, it enables a more efficient and structured encoding of motion with improved performance. Moreover, our functional formulation and skeleton-agnostic architecture naturally enable reconstruction from partial skeletons or incomplete temporal windows. We illustrate examples of temporal super-resolution in Figure Figure 4, and further validate this capability in the generation setting (5.2). In the Supplementary Materials, we provide additional experiments evaluating our model’s reconstruction when provided with progressively more incom-

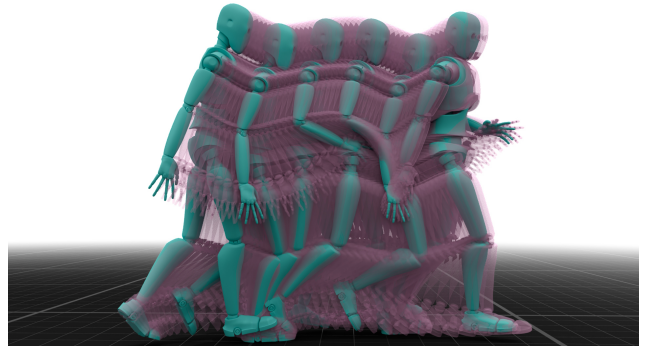


Figure 4. **FunPhase super-resolution.** Given a sparse set of keyframes, FunPhase reconstructs the full continuous motion while preserving physical plausibility.

plete temporal windows.

5.2. Latent diffusion in Phase Manifold

We perform diffusion directly in the phase manifold as described in 4.2. Quantitative results are reported in Table 2 for the human dataset 100STYLE and in Table 3 for the animal dataset ZOO. In the human case, the class conditioning is on locomotion style, while for animals on the species.

Overall, our approach achieves strong performance across both domains. Notably, our approach and the baseline *Function Diffusion* are the only methods that generate

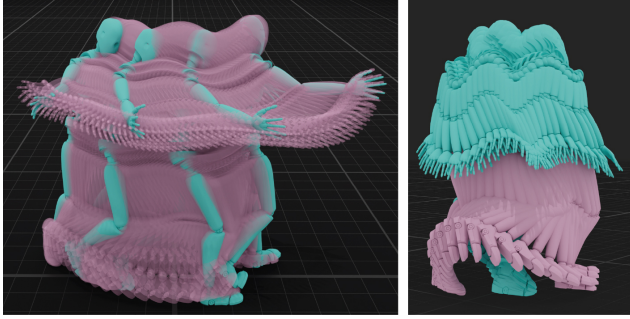


Figure 5. **Diffusion examples on 100STYLE.** On the left we show an example of generation from a sparse set of key frames (in green). On the right we show an example of body completion of the right leg (in pink).

motion in a *continuous functional space*. The key difference lies in our phase-formulation: by decomposing motion into phase components and applying the transformations in [Equation 9](#), FUNPHASE introduces temporal structure that significantly improves denoising stability and generation quality. As shown in [Table 2](#), this results in clear gains across all metrics.

Compared to state-of-the-art models such as CAMDM, ACMDM, and AnyTop, our method achieves the best or second-best results on nearly all metrics, particularly excelling in physics-based metrics. In particular, FUNPHASE achieves the lowest FID and foot-sliding error, indicating both high visual fidelity and superior physical realism. Beyond quantitative gains, our functional formulation enables generation under partial conditioning, such as from sparse keyframes or incomplete body observations. Examples of such scenarios are shown in [Figure 5](#).

Table 3. **Latent diffusion results on the ZOO dataset.** We compare our method with other multi-skeleton baselines.

Method	Cov. \uparrow	Div. \uparrow (Local)	Div. \uparrow (Inter)	Intra Div. \downarrow Diff.
SMDM [20]	89 ± 15	0.08 ± 0.13	0.28 ± 0.13	0.14 ± 0.09
AnyTop [6]	80 ± 22	0.26 ± 0.12	0.37 ± 0.18	0.14 ± 0.08
FunPhase	96 ± 7	0.11 ± 0.04	0.21 ± 0.05	0.06 ± 0.03

5.3. Motion Controller

To further validate the learned phase manifold, we train a Neural Motion Controller within our phase space following the setup of [\[26\]](#). The controller adopts a Weight-Blended Mixture-of-Experts architecture similar to [\[25, 36\]](#), but instead of relying on velocities or contact-based local phases as input to the gating network, it uses the phase vectors from our learned manifold ([Equation 2](#)). This design enables the model to generate motion in an autoregressive manner while

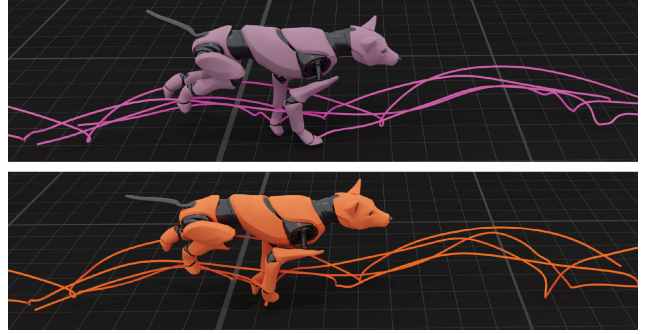


Figure 6. **Motion controller generation.** The top row shows the motion controller trained on FunPhase’s phase space, and the bottom row shows the controller trained on DeepPhase’s phase space. FunPhase enables the generation of smooth and realistic movements comparable to those produced by DeepPhase, highlighting the advantages of the phase manifold.

operating in a more expressive space than DeepPhase. The controller produces coherent motion sequences conditioned on both style and user inputs such as trajectories. Qualitative examples and a visual comparison with DeepPhase are presented in [Figure 6](#) and in the supplemental video.

5.4. Limitations

Although FunPhase demonstrates strong performance across reconstruction and generative tasks, there remains room for improvement in modeling longer frame windows under the super-resolution setting. The current formulation may lose fine-grained temporal detail when reconstructing motion at very low sampling rates. Additionally, while the learned phase manifold provides a strong inductive bias, the diversity of generated motions could be further enhanced through improved sampling strategies or richer conditioning mechanisms. Future work will explore these directions to strengthen both reconstruction fidelity and generative variability.

6. Conclusion and Future Work

We introduced FunPhase, a functional periodic autoencoder that learns a continuous phase manifold for motion. By representing motion as a spatio-temporal function, FunPhase unifies motion prediction and generation within a single interpretable framework and achieves high fidelity across diverse skeletons and datasets. Our results demonstrate that embedding periodic structure in function space improves reconstruction accuracy, physical plausibility, and denoising stability in diffusion-based generation.

A promising direction for future work involves integrating physics-based priors into the functional formulation, leveraging them to enhance realism and generalization. We also plan to explore further applications such as motion in-betweening and body-part motion completion, expand-

ing the practical scope of functional phase representations.

References

- [1] Armin Bruderlin and Lance Williams. Motion signal processing. In *Proceedings of the 22nd annual conference on Computer graphics and interactive techniques*, pages 97–104, 1995. [2](#)
- [2] Rui Chen, Mingyi Shi, Shaoli Huang, Ping Tan, Taku Komura, and Xuelin Chen. Taming diffusion probabilistic models for character control. In *ACM SIGGRAPH 2024 Conference Papers*, pages 1–10, 2024. [2, 6, 7](#)
- [3] Xin Chen, Biao Jiang, Wen Liu, Zilong Huang, Bin Fu, Tao Chen, and Gang Yu. Executing your commands via motion diffusion in latent space. In *Proceedings of the IEEE/CVF conference on computer vision and pattern recognition*, pages 18000–18010, 2023. [2, 6, 7](#)
- [4] Ke Fan, Shunlin Lu, Minyue Dai, Runyi Yu, Lixing Xiao, Zhiyang Dou, Junting Dong, Lizhuang Ma, and Jingbo Wang. Go to zero: Towards zero-shot motion generation with million-scale data. *arXiv preprint arXiv:2507.07095*, 2025. [2](#)
- [5] Giulio Franzese, Giulio Corallo, Simone Rossi, Markus Heinonen, Maurizio Filippone, and Pietro Michiardi. Continuous-time functional diffusion processes. *Advances in Neural Information Processing Systems*, 36:37370–37400, 2023. [3](#)
- [6] Inbar Gat, Sigal Raab, Guy Tevet, Yuval Reshef, Amit Haim Bermano, and Daniel Cohen-Or. Anytop: Character animation diffusion with any topology. In *Proceedings of the Special Interest Group on Computer Graphics and Interactive Techniques Conference Conference Papers*, pages 1–10, 2025. [2, 6, 8, 3](#)
- [7] Anand Gopalakrishnan, Ankur Mali, Dan Kifer, Lee Giles, and Alexander G Ororbia. A neural temporal model for human motion prediction. In *Proceedings of the IEEE/CVF Conference on Computer Vision and Pattern Recognition*, pages 12116–12125, 2019. [6, 2](#)
- [8] Tiankai Hang, Shuyang Gu, Chen Li, Jianmin Bao, Dong Chen, Han Hu, Xin Geng, and Baining Guo. Efficient diffusion training via min-snr weighting strategy. In *Proceedings of the IEEE/CVF international conference on computer vision*, pages 7441–7451, 2023. [2](#)
- [9] Daniel Holden, Taku Komura, and Jun Saito. Phase-functioned neural networks for character control. *ACM Transactions on Graphics (TOG)*, 36(4):1–13, 2017. [2, 3](#)
- [10] Andrew Jaegle, Felix Gimeno, Andy Brock, Oriol Vinyals, Andrew Zisserman, and Joao Carreira. Perceiver: General perception with iterative attention. In *International conference on machine learning*, pages 4651–4664. PMLR, 2021. [4](#)
- [11] Biao Jiang, Xin Chen, Wen Liu, Jingyi Yu, Gang Yu, and Tao Chen. Motiongpt: Human motion as a foreign language. *Advances in Neural Information Processing Systems*, 36:20067–20079, 2023. [2](#)
- [12] Aliasghar Khani, Arianna Rampini, Evan Atherton, and Bruno Roy. Unimogen: Universal motion generation. *arXiv preprint arXiv:2505.21837*, 2025. [2](#)
- [13] Aliasghar Khani, Arianna Rampini, Bruno Roy, Larasika Nadela, Noa Kaplan, Evan Atherton, Derek Cheung, and Jacky Biblioicwicz. Motion generation: A survey of generative approaches and benchmarks. *arXiv preprint arXiv:2507.05419*, 2025. [1, 3](#)
- [14] Nhat Le, Khoa Do, Xuan Bui, Tuong Do, Erman Tjiputra, Quang D Tran, and Anh Nguyen. Scalable group choreography via variational phase manifold learning. In *European Conference on Computer Vision*, pages 293–311. Springer, 2024. [2](#)
- [15] Peizhuo Li, Sebastian Starke, Yuting Ye, and Olga Sorkine-Hornung. Walkthedog: Cross-morphology motion alignment via phase manifolds. In *ACM SIGGRAPH 2024 Conference Papers*, pages 1–10, 2024. [2](#)
- [16] Zicheng Liu, Steven J Gortler, and Michael F Cohen. Hierarchical spacetime control. In *Proceedings of the 21st annual conference on Computer graphics and interactive techniques*, pages 35–42, 1994. [2](#)
- [17] Ian Mason, Sebastian Starke, and Taku Komura. Real-time style modelling of human locomotion via feature-wise transformations and local motion phases. *Proceedings of the ACM on Computer Graphics and Interactive Techniques*, 5(1):1–18, 2022. [3, 6, 1](#)
- [18] Zichong Meng, Zeyu Han, Xiaogang Peng, Yiming Xie, and Huaizu Jiang. Absolute coordinates make motion generation easy. *arXiv preprint arXiv:2505.19377*, 2025. [2, 6, 7, 3](#)
- [19] William Peebles and Saining Xie. Scalable diffusion models with transformers. In *Proceedings of the IEEE/CVF international conference on computer vision*, pages 4195–4205, 2023. [5](#)
- [20] Sigal Raab, Inbal Leibovitch, Guy Tevet, Moab Arar, Amit H Bermano, and Daniel Cohen-Or. Single motion diffusion. *arXiv preprint arXiv:2302.05905*, 2023. [2, 6, 8](#)
- [21] Tim Salimans and Jonathan Ho. Progressive distillation for fast sampling of diffusion models. *arXiv preprint arXiv:2202.00512*, 2022. [2](#)
- [22] Jiaming Song, Chenlin Meng, and Stefano Ermon. Denoising diffusion implicit models. *arXiv preprint arXiv:2010.02502*, 2020. [2](#)
- [23] Paul Starke, Sebastian Starke, Taku Komura, and Frank Steinicke. Motion in-betweening with phase manifolds. *Proceedings of the ACM on Computer Graphics and Interactive Techniques*, 6(3):1–17, 2023. [2](#)
- [24] Sebastian Starke, He Zhang, Taku Komura, and Jun Saito. Neural state machine for character-scene interactions. *ACM Transactions on Graphics*, 38(6):178, 2019. [2](#)
- [25] Sebastian Starke, Yiwei Zhao, Taku Komura, and Kazi Zaman. Local motion phases for learning multi-contact character movements. *ACM Transactions on Graphics*, 39(4), 2020. [2, 3, 8](#)
- [26] Sebastian Starke, Ian Mason, and Taku Komura. Deepphase: Periodic autoencoders for learning motion phase manifolds. *ACM Transactions on Graphics (ToG)*, 41(4):1–13, 2022. [2, 3, 4, 6, 7, 8](#)

[27] Guy Tevet, Sigal Raab, Brian Gordon, Yonatan Shafir, Daniel Cohen-Or, and Amit H Bermano. Human motion diffusion model. *arXiv preprint arXiv:2209.14916*, 2022. 2

[28] TrueBones. Truebones motion-capture dataset. <https://truebones.gumroad.com/l/skZMC>, 2025. Accessed: 2025-07-02. 6, 3

[29] Weilin Wan, Yiming Huang, Shutong Wu, Taku Komura, Wenping Wang, Dinesh Jayaraman, and Lingjie Liu. Difusionphase: Motion diffusion in frequency domain. *arXiv preprint arXiv:2312.04036*, 2023. 2

[30] He Wang, Edmond SL Ho, Hubert PH Shum, and Zhanxing Zhu. Spatio-temporal manifold learning for human motions via long-horizon modeling. *IEEE transactions on visualization and computer graphics*, 27(1):216–227, 2019. 2

[31] Sifan Wang, Zehao Dou, Tong-Rui Liu, and Lu Lu. Fundiff: Diffusion models over function spaces for physics-informed generative modeling. *arXiv preprint arXiv:2506.07902*, 2025. 2, 3, 4

[32] Xuan Wang, Kai Ruan, Xing Zhang, and Gaoang Wang. Animo: Species-aware model for text-driven animal motion generation. In *Proceedings of the Computer Vision and Pattern Recognition Conference*, pages 1929–1939, 2025. 2

[33] Yuyang Wang, Ahmed A Elhag, Navdeep Jaitly, Joshua M Susskind, and Miguel Angel Bautista. Swallowing the bitter pill: Simplified scalable conformer generation. *arXiv preprint arXiv:2311.17932*, 2023. 3

[34] Ye Wang, Sipeng Zheng, Bin Cao, Qianshan Wei, Weishuai Zeng, Qin Jin, and Zongqing Lu. Scaling large motion models with million-level human motions. In *Forty-second International Conference on Machine Learning*, 2025. 2

[35] Ye Yuan, Jiaming Song, Umar Iqbal, Arash Vahdat, and Jan Kautz. Physdiff: Physics-guided human motion diffusion model. 2023 ieee. In *CVF International Conference on Computer Vision (ICCV)*, pages 15964–15975, 2022. 2

[36] He Zhang, Sebastian Starke, Taku Komura, and Jun Saito. Mode-adaptive neural networks for quadruped motion control. *ACM Transactions on Graphics (ToG)*, 37(4):1–11, 2018. 6, 8

[37] Kaiwen Zheng, Cheng Lu, Jianfei Chen, and Jun Zhu. Improved techniques for maximum likelihood estimation for diffusion odes. In *International Conference on Machine Learning*. PMLR, 2023. 5

[38] Yi Zhou, C Barnes, J Lu, J Yang, and H Li. On the continuity of rotation representations in neural networks. 2019 ieee. In *CVF Conference on Computer Vision and Pattern Recognition (CVPR)*, 2018. 4

[39] Wentao Zhu, Xiaoxuan Ma, Dongwoo Ro, Hai Ci, Jinlu Zhang, Jiaxin Shi, Feng Gao, Qi Tian, and Yizhou Wang. Human motion generation: A survey. *IEEE Transactions on Pattern Analysis and Machine Intelligence*, 46(4):2430–2449, 2023. 2, 3, 6

FunPhase: A Periodic Functional Autoencoder for Motion Generation via Phase Manifolds

Supplementary Material

7. Implementation Details

This section provides additional implementation details and the experimental configurations. The code will be released upon publication.

7.1. FunPhase

Positional Encoding. To provide the model with information about temporal structure and skeletal topology, we employ two types of positional encodings:

(i) *Temporal Encoding*: We use Fourier positional encoding for temporal coordinates. For frame time t , we compute: $\mathbf{p}_t^{time} = [\sin(2\pi f_1 t), \cos(2\pi f_1 t), \dots, \sin(2\pi f_K t), \cos(2\pi f_K t)]$ where the frequencies f_k are geometrically spaced and K is the maximum number of frequencies.

(ii) *Spatial Encoding*: We encode skeletal topology using eigenvectors of the normalized graph Laplacian, providing information about joint connectivity and structural relationships. For a skeleton graph with adjacency matrix $\mathbf{A} \in \mathbb{R}^{J \times J}$ and degree matrix $\mathbf{D} \in \mathbb{R}^{J \times J}$, we compute the normalized Laplacian $\mathbf{L} = \mathbf{D}^{-1/2}(\mathbf{D} - \mathbf{A})\mathbf{D}^{-1/2}$ and use its first N eigenvectors as positional encodings $\mathbf{p}_j^{graph} \in \mathbb{R}^N$ for joint j , excluding the first constant eigenvector. In the case of the dataset composed of graphs with different sizes, we encode the skeletal graph structure using the graph heat diffusion operator $\mathbf{H}_t = e^{-t\mathbf{L}}$ at time $t > 0$. Let $\mathcal{T} = \{t_1, \dots, t_T\}$ be a set of heat diffusion times, and let $r^{(q)} \sim \mathcal{N}(0, I_N)$ for $q = 1, \dots, Q$ be random probe vectors. For each pair (t_i, q) , we compute the diffused signal $p_{t_i}^{(q)} = \mathbf{H}_{t_i} r^{(q)} = e^{-t_i \mathbf{L}} r^{(q)}$. The resulting spatial encoding is constructed by concatenating all diffused probes:

$$\mathbf{P}^{graph} = [p_{t_1}^{(1)}, \dots, p_{t_1}^{(Q)}, p_{t_2}^{(1)}, \dots, p_{t_T}^{(Q)}] \in \mathbb{R}^{J \times N}.$$

Architecture. In the largest model variant, which we use for the 100STYLE dataset [17], the architecture employs 256 latent channels, with separate encoders and decoders for joints and root. The joint encoder maps inputs to 256-dimensional embeddings and processes them through 5 Perceiver encoder blocks, each with depth 1. The root encoder uses 64 latents with 128-dimensional embeddings, processed through 3 encoder blocks with depth 1. Both decoders use 5 and 3 blocks respectively with depth 1. The model contains approximately $34M$ parameters. We use 60-frame motion clips (1 second at 60 fps), which we randomly subsample along both temporal and graph dimensions. At training time we use the AdamW optimizer with

a learning rate of $1e-4$. A cosine learning-rate schedule with warm-up and gradient clipping at 0.5 is applied.

7.2. Diffusion model

Our latent diffusion model takes as input a noisy phase-latent vector and a set of conditioning signals: diffusion timestep, class label, and partial motion input. The conditioning are embedded and concatenated in a single vector \mathbf{c} .

Backbone. The core architecture consists of:

- Linear Embedding: Projects each latent token from dimension 4 to embedding dimension $d_{embed} = 256$ to obtain a new latent representation \mathbf{h} .
- Positional Encoding: 1D sinusoidal positional embeddings provide positional information across the latent channels
- DiT Blocks: $L = 8$ transformer blocks with adaptive layer normalization (AdaLN) for conditioning
- Output Projection: Projects back to the latent dimension 4

Each DiT block employs adaptive layer normalization modulated by the conditioning signal:

$$\text{AdaLN}(\mathbf{h}, \mathbf{c}) = \gamma(\mathbf{c}) \odot \text{LayerNorm}(\mathbf{h}) + \beta(\mathbf{c})$$

where γ and β are scale and shift parameters predicted from the conditioning vector \mathbf{c} .

Conditioning Mechanism. The model is conditioned on three signals:

(i) *Timestep Embedding*: The diffusion timestep t is encoded via learned sinusoidal embeddings followed by an MLP:

$$\mathbf{e}_t = \text{MLP}(\text{SinusoidalEmbed}(t)) \in \mathbb{R}^{256}.$$

(ii) *Class Embedding*: Motion class labels $y \in \{1, \dots, K\}$ are embedded via a learned embedding layer:

$$\mathbf{e}_y = \text{Embed}(y) \in \mathbb{R}^{64}.$$

(iii) *Partial Motion*: Optionally, a subset of joint rotations and root positions can be provided as conditioning input. These are encoded through the FunPhase encoder, and the resulting latent vector is then embedded via a learned embedding layer:

$$\mathbf{e}_{context} = \text{Embed}_{context}(D_{FunPhase}([\tilde{\mathbf{R}}; \tilde{\mathbf{X}}^{root}])) \in \mathbb{R}^{256}.$$

These embeddings are concatenated and projected to form the conditioning vector:

$$\mathbf{c} = \text{MLP}([\mathbf{e}_t; \mathbf{e}_y; \mathbf{e}_{context}]) \in \mathbb{R}^{256}.$$

Training Objective. We adopt the v -parameterization objective [21], which predicts the velocity rather than noise or clean signal. The velocity target is defined as:

$$\mathbf{v}_t = \sqrt{\bar{\alpha}_t} \boldsymbol{\epsilon} - \sqrt{1 - \bar{\alpha}_t} \mathbf{z}_0$$

where \mathbf{z}_0 is the clean latent code, $\boldsymbol{\epsilon} \sim \mathcal{N}(\mathbf{0}, \mathbf{I})$ is Gaussian noise, and $\bar{\alpha}_t$ is the cumulative product of noise schedule coefficients at timestep t .

The noisy latent at timestep t is computed as:

$$\mathbf{z}_t = \sqrt{\bar{\alpha}_t} \mathbf{z}_0 + \sqrt{1 - \bar{\alpha}_t} \boldsymbol{\epsilon}$$

Given \mathbf{v}_t , we can recover both the noise and clean signal:

$$\begin{aligned} \mathbf{z}_0 &= \sqrt{\bar{\alpha}_t} \mathbf{z}_t - \sqrt{1 - \bar{\alpha}_t} \mathbf{v}_t \\ \boldsymbol{\epsilon} &= \sqrt{\bar{\alpha}_t} \mathbf{v}_t + \sqrt{1 - \bar{\alpha}_t} \mathbf{z}_t \end{aligned}$$

Loss Function. The training objective is:

$$\mathcal{L}_{diff} = \mathbb{E}_{\mathbf{z}_0, t, \boldsymbol{\epsilon}, y} [\lambda_t \|\mathbf{v}_t - \mathbf{v}_\theta(\mathbf{z}_t, t, y)\|_2^2]$$

where $t \sim \mathcal{U}(1, T)$ is uniformly sampled from $[1, 1000]$, and λ_t is a weighting term.

Min-SNR Loss Weighting. We employ minimum signal-to-noise ratio (SNR) loss weighting [8] to balance learning across different noise levels:

$$\lambda_t = \min \left(\frac{\bar{\alpha}_t}{1 - \bar{\alpha}_t}, \gamma \right)$$

where $\gamma = 5$ is a hyperparameter that prevents over-weighting low-noise timesteps.

Noise Schedule. We use a linear beta schedule:

$$\beta_t = \beta_{\min} + \frac{t}{T} (\beta_{\max} - \beta_{\min})$$

with $T = 1000$ total diffusion steps, $\beta_{\min} = 0.0001$, and $\beta_{\max} = 0.02$.

Sampling Procedure. For generation, we employ Denoising Diffusion Implicit Models (DDIM) [22], which enables high-quality sampling with fewer steps than the training schedule.

Starting from pure noise $\mathbf{z}_T \sim \mathcal{N}(\mathbf{0}, \mathbf{I})$, we iteratively denoise:

$$\mathbf{z}_{t-1} = \sqrt{\bar{\alpha}_{t-1}} \hat{\mathbf{z}}_0 + \sqrt{1 - \bar{\alpha}_{t-1} - \sigma_t^2} \cdot \hat{\boldsymbol{\epsilon}} + \sigma_t \boldsymbol{\epsilon}_t$$

where: - $\hat{\mathbf{z}}_0 = \sqrt{\bar{\alpha}_t} \mathbf{z}_t - \sqrt{1 - \bar{\alpha}_t} \hat{\mathbf{v}}_t$ is the predicted clean latent - $\hat{\boldsymbol{\epsilon}} = \sqrt{\bar{\alpha}_t} \hat{\mathbf{v}}_t + \sqrt{1 - \bar{\alpha}_t} \mathbf{z}_t$ is the predicted noise - $\sigma_t = \eta \sqrt{(1 - \bar{\alpha}_{t-1}) / (1 - \bar{\alpha}_t)} \sqrt{1 - \bar{\alpha}_t / \bar{\alpha}_{t-1}}$ controls stochasticity - $\eta = 1.0$ determines the interpolation between DDIM ($\eta = 0$) and DDPM ($\eta = 1$) - $\boldsymbol{\epsilon}_t \sim \mathcal{N}(\mathbf{0}, \mathbf{I})$ is fresh noise

	Joint Pos.	Rotation	Root Pos.
Unified	3.37	0.42	0.92
No FK Loss	26.8	0.097	0.65
32 Channels	5.68	0.65	2.11
128 Channels	4.01	0.52	1.57
256 Channels	3.15	0.092	0.86

Table 4. **FunPhase Ablation.** We test the performance of different architecture choices. The model 256 Channels represent our final model.

We use $S = 900$ sampling steps (out of $T = 1000$ training steps) for generation, with the timestep schedule:

$$\{t_s\}_{s=0}^S = \left\{ \left\lfloor \frac{sT}{S} \right\rfloor \right\}_{s=0}^S$$

Training. The diffusion model contains approximately 10M parameters and is trained for 100 epochs using the AdamW optimizer with learning rate 1×10^{-4} , $\beta_1 = 0.9$, $\beta_2 = 0.999$, and weight decay of 0.01. We use gradient clipping at norm 0.5 and a batch size of 64. The FunPhase autoencoder is frozen during diffusion training. All experiments are conducted on 4 NVIDIA A100 GPUs using PyTorch Lightning with mixed precision (FP16) training.

7.3. Metrics

Evaluating motion generation and reconstruction is notoriously challenging due to the need to jointly assess spatial accuracy, temporal coherence, physical plausibility, and perceptual realism [39]. Following standard practice, we employ a diverse set of metrics to ensure a fair and comprehensive evaluation. Visual examples are provided in the supplemental video. As reconstruction metrics, we use the *Joint Position Error (L2)*, measuring the average Euclidean distance between predicted and ground-truth joint positions; the *Geodesic Rotation Error* (Equation 4 in main paper), the mean angular distance between predicted and target joint rotations; and the *Normalized Power Spectral Similarity (NPSS)* [7], comparing the frequency-domain spectra of predicted and reference motions. We evaluate the physical plausibility of generated motion using: *Foot Sliding*: average velocity of grounded feet, measuring temporal drift artifacts; *Foot Penetration*: the mean vertical penetration of the feet below the ground plane; *Average Curve Length (ACL)*: mean joint acceleration magnitude, assessing temporal smoothness; *Coherence*: global consistency of joint trajectories over time. To assess generation quality, we use a pretrained motion classifier from [2] to compute the *Fréchet Inception Distance (FID)* between real and generated feature distributions, and classification *Accuracy* to measure the alignment of generated motions with the intended class

Table 5. **Input representation comparison on the 100STYLE dataset.** Representing motions using joint rotations and the root position yields consistently better performance than using global joint positions across almost all evaluation metrics.

Representation	Method	Position (cm) \downarrow	Orientation \downarrow	NPSS \downarrow	Sliding \downarrow	Penetration \downarrow	ACL \downarrow
GLOBAL POSITIONS	Function AE-128C	1.82	0.24	1.95	0.24	0.004	1.371
	FunPhase-32C	3.66	0.26	2.17	0.48	0.037	1.346
	FunPhase-128C	2.99	0.25	2.05	0.37	0.022	1.369
ROTATIONS + ROOT POSITION	Function AE-256C	<u>0.74</u>	0.05	0.59	0.23	0.001	1.383
	FunPhase-32C	1.93	<u>0.10</u>	1.18	0.16	0.001	1.371
	FunPhase-256C	0.36	0.20	<u>0.75</u>	<u>0.21</u>	0.001	1.378

condition. Finally, the *Diversity* is quantified as the average standard deviation among generated pose vectors across multiple samples per condition. On the TRUEBONES ZOO dataset [28], we follow the evaluation protocol of AnyTop [6]: *Coverage* quantifies how much of the real motion distribution is captured by the generated samples; *Local Diversity* measures the average distance between short windows in generated motions and their nearest neighbors in the ground truth; *Inter Diversity* captures variation across different generated motions, while *Intra Diversity Diff* reports the difference in within-motion diversity between generated and ground-truth sequences.

8. Ablations

In this section, we show the ablation studies that guided our final model design.

8.1. FunPhase

We trained the ablation models using 20% of the 100STYLE training set for 60 epochs.

Model size. We first ablate the number of latent channels in FunPhase. Table 4 reports the reconstruction errors for models with 32, 128, and 256 channels. As expected, the largest variant achieves the best performance across all metrics. Notably, even this configuration remains extremely compact, using only 256×4 values per motion clip.

Root position encoding. We also evaluate a unified architecture that uses a single encoder to handle both joint rotations and the root position. In this setup, the root is treated as an additional node with a zero-valued graph positional encoding. We train this model with 256 latent channels and refer to it as *Unified*. As shown in Table 4, our final model (with separate encoders and decoders) consistently outperforms *Unified* across all metrics. Moreover, keeping the root and joint inputs separate allows finer control over computational resources allocated to global versus local information.

Forward Kinematic Loss. Finally, we assess the impact of the forward kinematic loss in training. Removing this term (*No FK Loss*) results in a substantial drop in per-

formance, as reported in Table 4. This confirms that the forward kinematic loss is essential for reconstructing physically plausible motion.

8.2. Motion representation

Previous work has shown that directly predicting global joint positions can be advantageous for generative models [18]. However, for our model we adopt joint rotations together with the root position as the motion representation. This choice avoids skeletal deformations and is directly compatible with standard animation software. Given a fixed skeleton, global joint positions can be efficiently obtained through forward kinematics. In contrast, predicting global positions directly may introduce errors caused by inconsistent bone lengths across frames. Moreover, converting predicted global positions back into local joint rotations—required by common motion-capture formats such as BVH—necessitates an inverse-kinematics optimization step, which is substantially more expensive than forward kinematics.

This choice is further supported by the results of our ablation in Table 5. We trained both FunPhase and Function AE on the full 100STYLE dataset using the global joint positions, reducing the latent channels to 128 to match the smaller dimensionality of this representation. We also present results using 32 latent channels in both cases, to ensure a fair comparison. The results show that jointly predicting rotations and root position achieves lower reconstruction error, indicating that global joint coordinates are not advantageous for our task.

Table 6. **Phase Transformation Ablation.** Comparison between the Diffusion Latent Model with and without Phase Transformation.

Phase Transf.	FID \downarrow	Accuracy (%) \uparrow	Diversity \uparrow
No	1.28 ± 0.44	34.83	0.56 ± 0.01
Yes	1.27 ± 0.48	37.6	0.56 ± 0.01

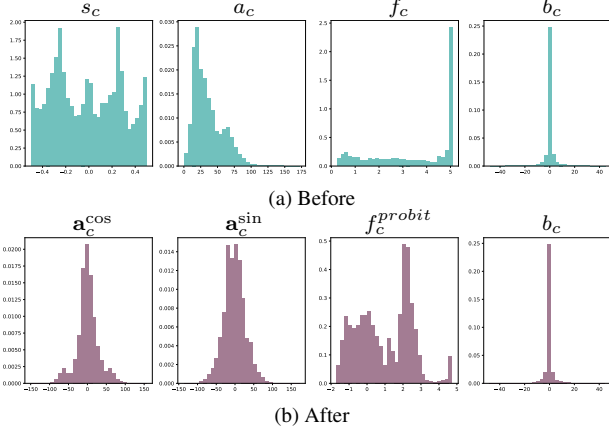


Figure 7. **Phase Transformation.** We plot the distribution of the latent periodic parameterization before and after the phase transformation applied in the latent diffusion model.

8.3. Phase Transformation

The periodic parameterization, while compact and interpretable, poses challenges for diffusion modeling due to the domain and distribution of its parameters. To address this, we apply domain transformations that make the representation more compatible with Gaussian diffusion. Figure 7 illustrates how the Phase Transformation described in Equation 9 of the main manuscript reshapes the distribution of the latent phase parameters. The resulting distributions more closely resemble a Normal distribution, which is known to facilitate the diffusion process [].

To evaluate its benefits, we train Latent Diffusion models (with and without the Phase Transformation) using 2M parameters on a 20% subset of the 100STYLE training set. As shown in Table 6, adding the Phase Transformation improves performance under these conditions. Furthermore, the effectiveness of phase parameterization in latent diffusion is reinforced by the substantial performance gains observed when comparing Function Diffusion with our FunPhase Diffusion in Table 1 of the main paper.

KF Dist.	25	15	10	5
SLERP	14.79	4.11	1.32	0.43
Function AE	126.21	6.02	1.29	0.76
FunPhase	151.24	11.61	0.99	0.39

Table 7. **Reconstruction error under decreasing keyframe distances.** Given a fixed window of 50 frames, each model reconstructs the full motion from a subsampled set of keyframes. FunPhase provides more accurate interpolation than both standard autoencoders and linear interpolation (SLERP) at shorter intervals.

9. Reconstruction error under increasing keyframe distances.

In Table 7, we evaluate the reconstruction performance of our model when conditioned on keyframes sampled at increasing temporal intervals. We compare Function AE and FunPhase against a SLERP baseline, which linearly interpolates the root trajectory and joint rotations between keyframes. FunPhase shows a substantial improvement at a keyframe distance of 10 and nearly matches full-sequence reconstruction performance at a distance of 5.